Advanced Sensors and Instrumentation

Issue 15 • September 2021

ASI Program Update

Daniel Nichols
Department of Energy

Pattrick Calderoni
Idaho National Laboratory

The Advanced Sensor and Instrumentation (ASI) program has completed its 10th year since implementation in Fiscal Year 2011. Despite the continued challenges caused by the COVID-19 pandemic, the program has achieved remarkable accomplishments in the development of Instrumentation and Control (I&C) technologies, some of which are highlighted in this newsletter. The focus of the program strategy towards the demonstration of mature technologies in response of stakeholder's needs has begun to provide the anticipated crosscutting impact that is the foundation of the program's mission. This fiscal year has seen a renewed effort to coordinate the program priorities with Department of Energy (DOE) industrial partners, in particular companies developing advanced reactor concepts. This will strengthen the adoption of ASI technologies in advanced reactor designs and their demonstration, maximizing the program impact on DOE Office of Nuclear Energy's (NE) activities.

The ASI program welcomes a new program manager to the team. Daniel Nichols has taken over Melissa Bates' responsibilities as the DOE-NE headquarters' program manager. Nichols grew up in Kansas, attending Kansas State University (KSU) to obtain his B.S. in Mechanical Engineering and his Ph.D. in Nuclear Engineering. During his time at KSU, his graduate research focused on the development of a small form factor neutron flux monitoring device, known as the Micro-Pocket Fission Detector. He also worked on research relating to reactor core modeling for accident tolerant fuels, gamma-ray spectroscopy of irradiated fuel elements, and neutron detector platforms designed for non-proliferation and special nuclear materials monitoring. Throughout his undergraduate and graduate degree, he worked part time at the KSU TRIGA Mark II Nuclear Research

Continued on next page

In this issue...

1. ASI Program Update..... p. 1
2. Magnetostrictive Ultrasonic Transducer for In-Pile Thermometry..... p. 3
3. Optical fiber DTS measurement in DRIFT heat sink.... p. 6
4. Self-Powered Neutron Detector Testing and Characterization in Test Reactors..... p. 9
5. Impedance sensor development..... p. 12
6. Development of an Optical Fiber Based Gamma Thermometer ..... p. 15
7. Analytics-at-scale of Sensor Data for Digital Monitoring in Nuclear Plants ..... p. 18
8. Zero-Group-Velocity method for microstructure characterization ..... p. 21

For more program information, including recent publications, please visit www.energy.gov/ne

U.S. DEPARTMENT OF ENERGY

Continued from previous page

Reactor and obtained his Reactor Operator and Senior Reactor Operator licenses from the Nuclear Regulatory Commission. While completing his graduate degree, he gained national laboratory experience as an intern at Idaho National Laboratory helping deploy and test advanced sensors at both the Transient Reactor Test Facility and the Advanced Test Reactor Critical Facility. These experiences provided him technical expertise in sensor development with a perspective from both the university and national laboratory levels. As the program manager for the ASI program, Nichols envisions growing the program's relationship with industry partners through frequent discussions to understand customer needs and provide feedback to better tailor research project goals. One of his main focuses for the program is to develop and compile a robust portfolio of sensors, instrumentation and controls technologies that are readily available for adoption by the existing reactor fleet, material test reactors, and advanced reactors. He is proud to be working with the ASI team and looks forward to guiding the program and collaborating with researchers to achieve successful outcomes for advancing the DOE-NE mission.

Magnetostrictive Ultrasonic Transducer for In-Pile Thermometry

Joshua Daw
Idaho National Laboratory

Zhangxian (Dan) Deng
Boise State University

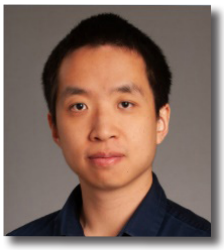

Introduction

Monitoring fuel rod temperatures are important to measure reactor core performance and ensure reactor system integrity throughout operation. Current methods for in-core temperature measurement include passive melt wires or paint spots that only provides sparse temperature data points, thermocouples that exhibit thermal drift and short lifespan, and linear variable differential transformer (LVDT) expansion thermometers whose measurement range is constrained by coil insulation and LVDT core's Curie temperature [1-2].

Ultrasonic Thermometry Background

Ultrasonic thermometry (UT) based on magnetostrictive waveguides is a promising alternative to existing temperature measurement methods [3]. Figure 1 illustrates the working principle of a UT in which a transceiver simultaneously generates ultrasonic pulses and receives resulting acoustic reflections. By measuring the time of flight of selected reflections, we can quantify the speed of sound, derive the Young's modulus of the waveguide; therefore, temperature values can be identified at each section. A DC magnetic field provided by a permanent magnet or a solenoid is necessary to bias the magnetostrictive waveguide and maximize the signal-to-noise ratio.

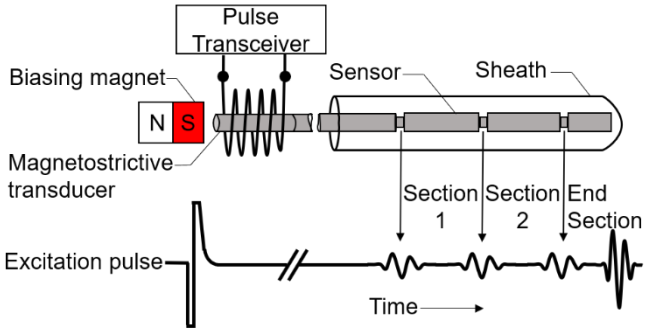

Figure 1. Schematic of ultrasonic waveguide thermometry. (adapted from Laurie et al., 2010)

To further accommodate the design requirements associated with nuclear applications, we chose iron-gallium alloys, also known as Galfenol, as the waveguide material candidate [4-6]. Galfenol remains stable after 8.68E20 n/cm^2 of accumulated neutron fluence. The Curie and melting temperatures for Galfenol is 700°C and 1450°C, respectively. Galfenol exhibits large magnetostriction up to 400 ppm.

Despite its great potential, the deployment of Galfenol UT is currently constrained by the complexity in signal analysis. We have noticed significant wave dispersion and detected measurement noises arising from shear modes or electromagnetic dynamics in the pulse transceiver. INL has recently laser-welded stainless steel waveguides to magnetostrictive wires to target higher fuel rod measurement. The reflections occurring at the interface of two dissimilar waveguides further complicate the signal analysis. To facilitate UT signal analysis, our research team developed and validated a multiphysics finite element model incorporating mechanical, magnetic, and/or thermal dynamics in UT.

Ultrasonic Waveguide Experiment

We first designed an experiment, as shown in Figure 2(a), to collect preliminary wave propagation data for model validation. A DC coil, an AC coil, and a Galfenol waveguide were assembled coaxially. The DC coil generates a bias magnetic field driving the Galfenol waveguide to its burst region, where the magneto-mechanical coupling is the most significant.

Continued on next page

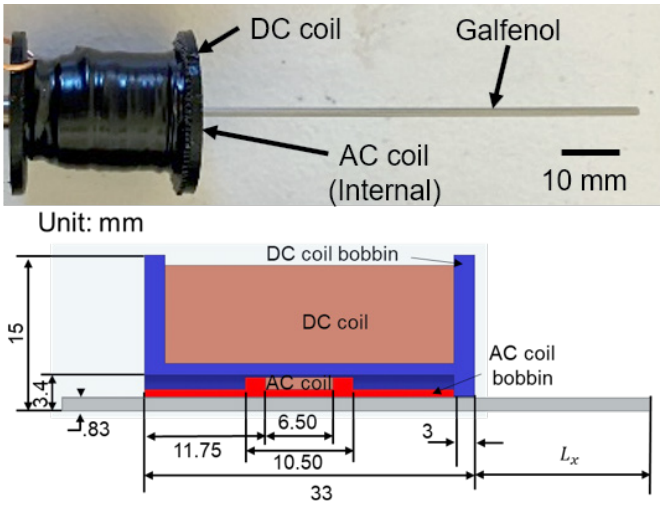

Figure 2. (a) physical assembly and (b) schematic (cross section view) of the waveguide transducer.

Continued from previous page

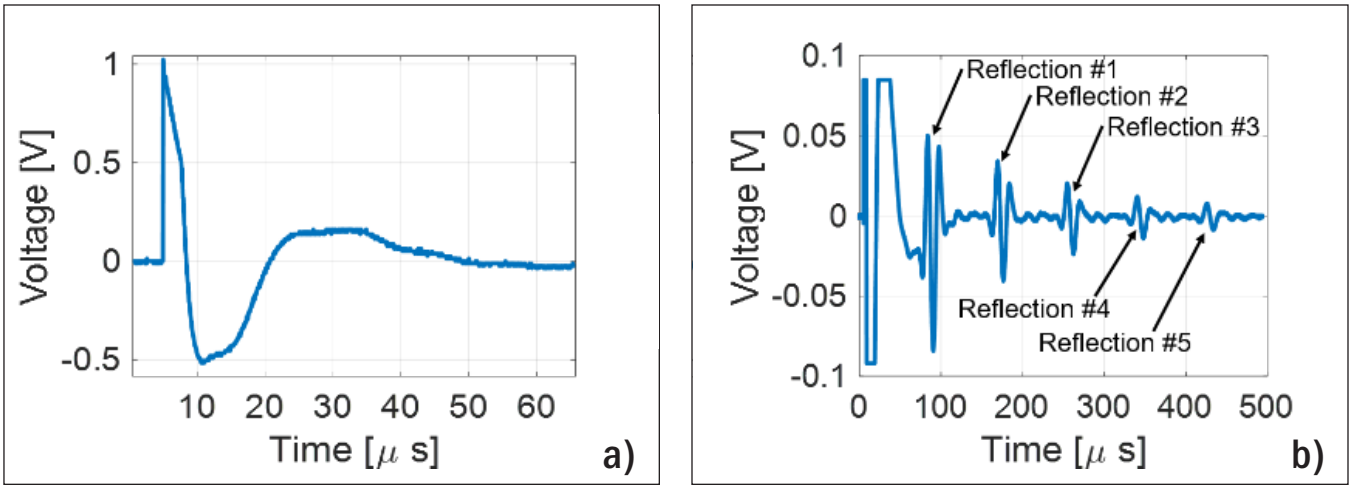

Figure 3. Experimental response for a) first 60 µs and b) up to 500 µs.

A 5-µs wide, 100-V magnitude square impulse voltage was applied to the AC coil, which excited the 100-kHz compressive mode of the Galfenol waveguide. Figure 3 shows the voltage measured across the AC coil. Since the AC excitation coil behaves like an inductor, we saw transient electrical dynamics that affect the response for the first 100 µs. To eliminate the impact of electrical dynamics, time of flight and speed of sound were derived using the 2nd and 5th reflections.

Ultrasonic Waveguide Simulation

A 2D axisymmetric model, as shown in Figure 2(b), was constructed in COMSOL Multiphysics. Modules for the mechanical, magnetic, and magnetostrictive domains were initialized. Classic Rayleigh damping coefficients were applied to the Galfenol waveguide.

To achieve optimal magneto-mechanical coupling and maximize the signal-to-noise ratio of the transducer, the DC coil needs to generate a magnetic field driving the Galfenol waveguide to the center of its burst region. According to previous characterization curves of Galfenol, the desired bias magnetic flux density level is approximately 0.8 T. Therefore, we first conducted a stationary parametric study by varying the current level applied to the DC coil. As shown in Figure 4, the magnetic field strength in the center of the AC coil achieved 0.7–0.8 T when a DC current of 1.0 A was applied. This matches the experimental results.

We then completed a time-dependent simulation to reproduce the voltage across the AC coil over time. The experimental and simulated results are overlaid in Figure 5.

Overall, the simulated model matches the experimental result well. However, the inductance of the AC excitation coil produced a transient period of electrical dynamics

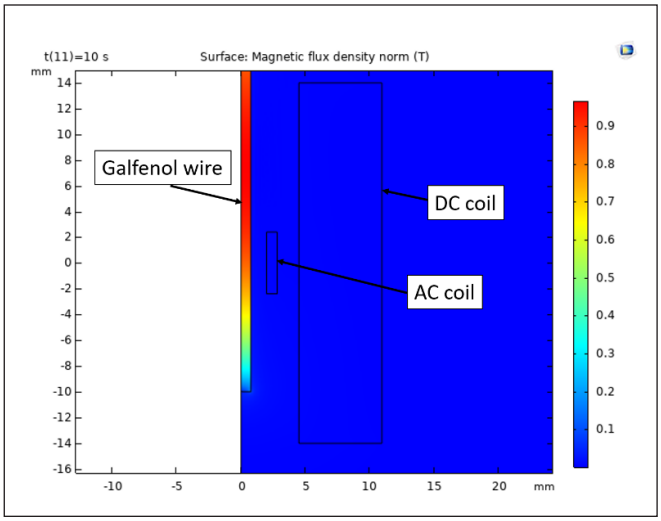

Figure 4 Magnetic flux density distribution when a DC current of 1.0 A was applied to the DC coil.

Continued on next page

Continued from previous page

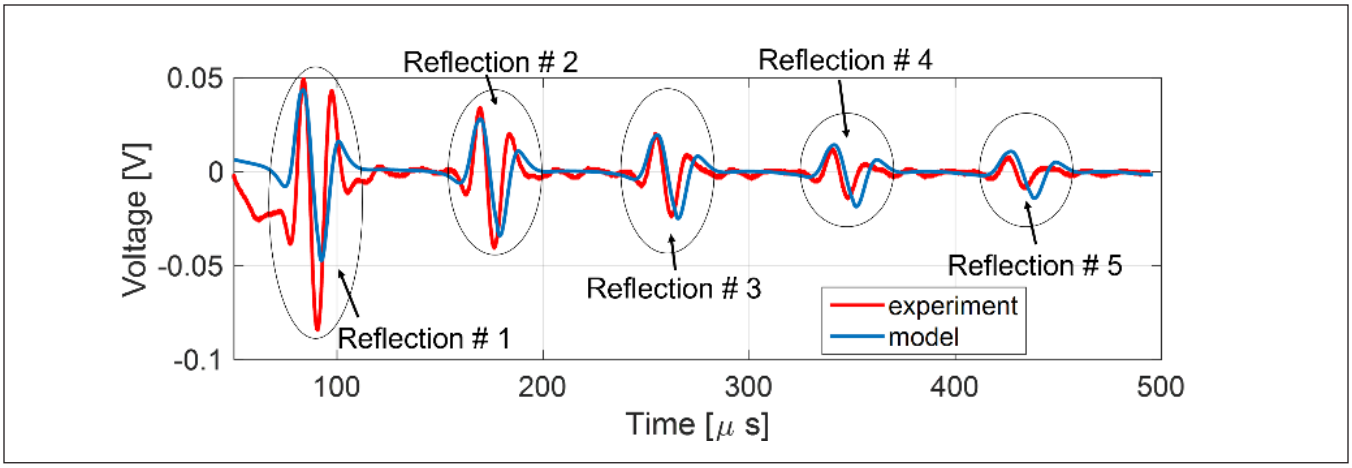

Figure 5. Comparison of simulation and experimental results.

(before 100 µs). The negligence of this transient state in the simulation resulted in a large discrepancy in the first reflection. The model is also less damped compared to the experimental result. This can be attributed to the fact that magnetic hysteresis and Joule heating energy losses were neglected in the simulation.

Future Work

Going forward, we will verify the UT thermometry by measuring its time of flight at elevated temperatures. We will use a laser vibrometer to directly measure the wave propagation for model validation. By including electrical dynamics and magnetic hysteresis, we will further mitigate the discrepancy between experimental results and simulation.

References

1. Kim, B. G., J. L. Rempe, J.-F. Villard, and S. Solstad. 2011. "Review of instrumentation for irradiation testing of nuclear fuels and materials." *Nuclear Technology* 176, no. 2: 155.

2. Knudson, D., J. Rempe, and J. Daw. 2009. *Evaluation of Candidate Linear Variable Displacement Transducers for High Temperature Irradiations in the Advanced Test Reactor*. INL/EXT-09-16972, Idaho National Laboratory (INL).

3. Laurie, M., et al. 2010. "Ultrasonic high-temperature sensors: past experiments and prospects for future use," *International Journal of Thermophysics* 31, no. 8-9, 1417.

4. Daw, J., B. Tittmann, and B. Reinhardt. 2016. "Ultrasonic Transducers for Harsh Environments," *IEEE International Ultrasonics Symposium (IUS)*: 1-3, doi: 10.1109/ULTSYM.2016.7728389.

5. Daw, J., et al. 2015. "Ultrasonic Transducer Irradiation Test Results," INL/CON-14-31882. Idaho National Laboratory (INL).

6. Daw, J. E., J. L. Rempe, and S. C. Wilkins. 2010. "Ultrasonic thermometry for in-pile temperature detection." INL/CON-10-18293. Idaho National Laboratory (INL).

Optical Fiber DTS Measurement in DRIFT Heat Sink

Kelly McCary
Idaho National Laboratory

Austin Fleming
Idaho National Laboratory

Introduction

The Nuclear Energy Enabling Technologies (NEET) Advanced Sensors and Instrumentation (ASI) program has supported the development of optical fiber distributed temperature sensors (DTS) for several years. The work included testing various fibers and configurations in the Transient Reactor Test Facility (TREAT), the development of packaging and feedthrough solutions, as well as a calibration process. Previous work evaluated the feasibility of deploying optical fiber DTS in-pile and tested solutions to expand the use cases for optical fiber sensors. A Dry In-Pile Fracture Test (DRIFT) capsule was designed and used in an experiment test campaign in TREAT. The DRIFT experiment is designed to serve two purposes: (1) validate fuel pellet cracking models developed as part of the MOOSE/BISON/MARMOT code package, and (2) compare pellet cracking behavior of a novel fuel design to that of standard fuel pellets [1]. The DRIFT experiment series included a calibration capsule and four test capsules that were irradiated in TREAT. This test series is the first deployment of an optical fiber DTS to meet a data objective for an experiment in TREAT. Fiber-optic-based instrumentation is a versatile and developing class of instruments for in-pile deployment. The successful deployment of optical fiber sensors requires the consideration of radiation-specific challenges, such as radiation-induced attenuation and radiation-induced emission, and sensor design considerations. Advances in radiation resistant fibers as well as previous research testing optical sensors in TREAT has led to successful deployments of various types optical sensors to meet data objectives in fueled experiments. This is the first deployment of the Optical Frequency Domain Reflectometry (OFDR) sensing technique.

Background

OFDR is an intrinsic sensing mechanism that allows for distributed temperature measurements to be made along the length of the fiber at sub-centimeter resolution. The OFDR technique operates on the principle of injecting light into an optical fiber and measuring the backscattered light (Rayleigh scatter) off the local density fluctuations along the length of the fiber. As the temperature increases, the optical fiber expands and the backscatter profile changes. This change can then be correlated to a change in temperature [2]. This method can also be used to measure strain distributed along the length of the fiber, where strain causes the fiber to expand or contract.

Deployment of a optical fiber DTS in an experiment requires much more development than deployment in a laboratory setting. There are many considerations that go into the development and fabrication of a sensor, including temperature requirements, required connections and feedthroughs, sensor termination, strain and vibration effects, radiation effects, and calibration considerations. Solutions to some in-pile specific concerns were addressed in previous work found in [3–5]. Sensor performance is dependent on the configuration of the deployment as well as the termination of the sensor and feedthroughs. Additional out-of-pile testing was conducted to characterize the functional ranges of the sensors [6]. Research is still ongoing to expand the operation range of optical fiber DTS,

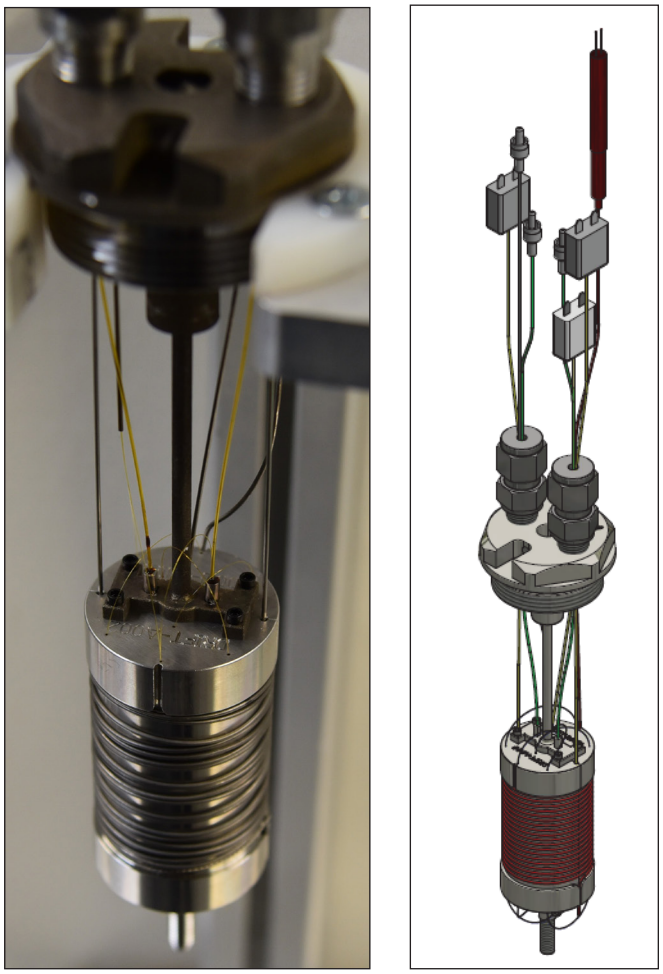

Figure 1. Photo of fully assembly DRIFT heat sink (left) and computer-aided design (CAD) model of the assembly (right).

Continued on next page

Continued from previous page

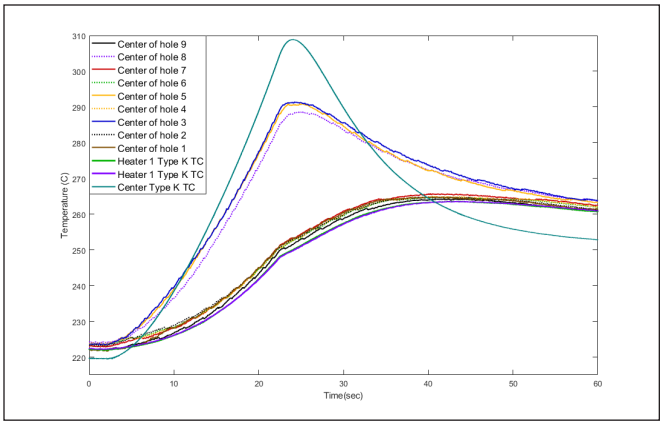

Figure 2. Temperature of the heat sink at the axial center of each hole and the temperature measured by the type-K thermocouples.

including work on higher temperature and more radiation-resistant feedthroughs and higher temperature fiber coatings.

The DRIFT experiment design consisted of an instrumented stainless-steel heat sink with fuel pellets in the center. The DTS fiber was woven through nine small holes that were electrical discharge machined (EDM) in the heat sink. The experiment also had three thermocouples (one in the fuel and two on the edges of the heat sink) and two optical pyrometers that measured the surface temperature of the fuel. Figure 1 shows a fully assembly DRIFT heat sink and computer-aided design (CAD) model of the assembly. A heater cable was wrapped around the outside of the heat sink to pre-heat the experiment to the desired temperature. During the experiment, the fuel pellets and heat sink are heated via the initial warming with the cable heater and then through fission when the reactor pulses. The heat sink is designed to replicate the heat removal from the fuel that would take place from the cooling in a light water reactor (LWR). As the temperature in the heat sink increases, the heat flux from the fuel decreases, the location of the holes in the heat sink were spaced to provide information about the axial, radial, and azimuthal temperature distribution in the heat sink with a single optical fiber [1]. The locations of the holes for the DTS fiber are shown in Figure 3, the fiber was routed into Hole 9 from the top and the through each hole in reverse numerical order such that Hole 1 was at the end of the fiber and Hole 9 was closest to the connector.

Results

The DTS fiber measured temperature every 1.3 mm along the entire length of the fiber. This allowed for 59 measurements axially in each hole in the heat sink as well as measurements of the air temperature above and below the heat sink. Figure 2 shows the response of the fiber at

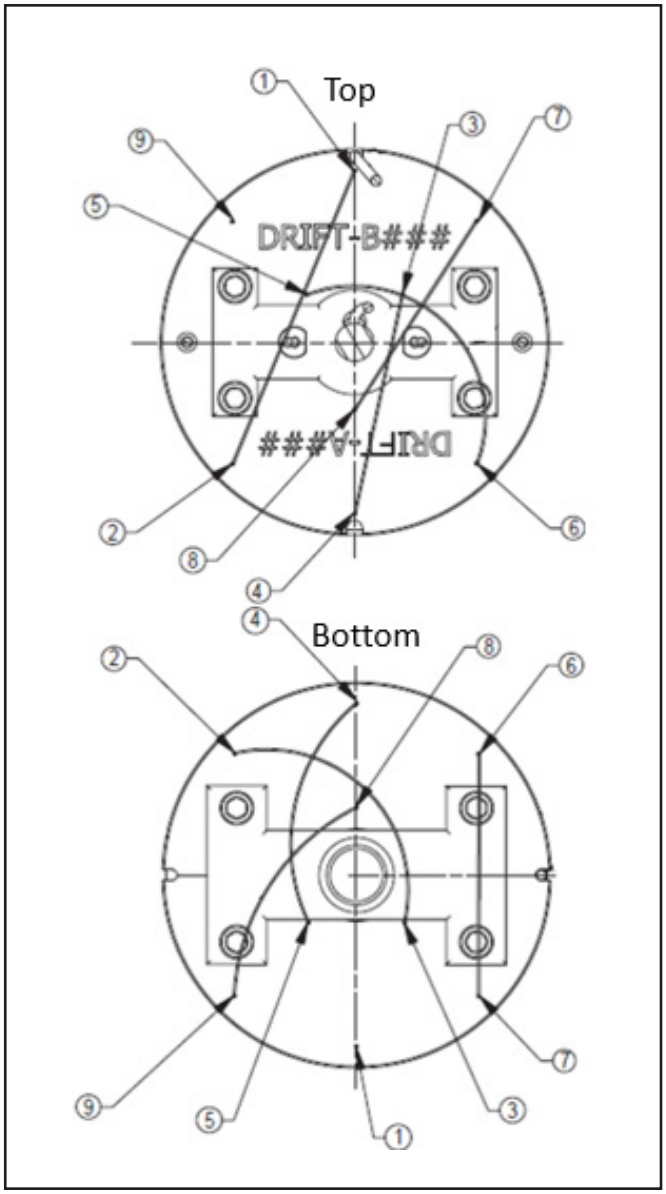

Figure 3. Location and routing sequence of the DTS fiber through the heat sink.

the center location of each hole in the heat sink and the thermocouple responses. Figure 4 shows the response along the entire length of the fiber at various times. The measured temperature by the fiber in the holes further from the fuel, The temperature measured by the fiber in the holes furthest from the fuel, agree well with the temperatures measured by the nearby heater thermocouples. The hole locations closer to the fuel reach a higher peak temperature during and immediately after the reactor transient than the outer holes, there may be some slight delay in the temperature measurement due to the air gap surrounding the fiber.

Continued on next page

Continued from previous page

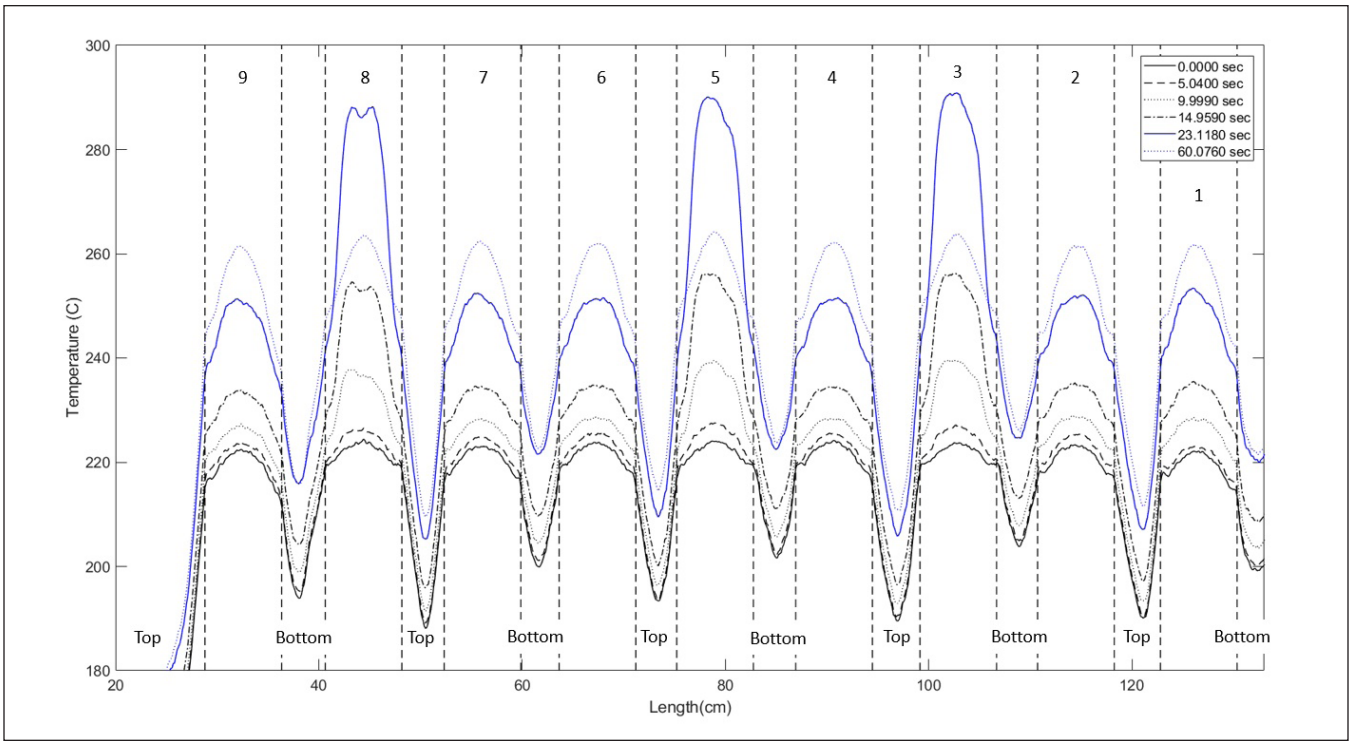

Figure 4. Temperature of heat sink and air gaps as measured by the DTS fiber.

Slowly all locations in the heat sink reach equilibrium through conduction as expected. The temperature data along the length of the fiber in Figure 4 shows more detail about the response of the heat sink. Specifically, the heat loss from the ends of the cylinder heat sink can be seen by the reduced temperature at the top and bottom of the heat sink prior to the transient in the DTS measurement.

Conclusions

Development of an optical fiber DTS led to a high spatial resolution measurement of the temperature in the DRIFT heat sink. To achieve the same density of measurements with conventional thermocouples, the necessary feedthrough would be prohibitive and the thermal response of the heat sink would be changed significantly. The small mass and diameter of the fiber allows for the temperature measurements to be taken without drastically changing the thermal properties of the heat sink itself. Future work includes expanding the applicable temperature range of the DTS fiber by testing and demonstrating higher temperature fiber coatings. While the optical fiber itself can withstand higher temperatures, installing an uncoated fiber in most experiment configurations is impractical and has a high risk of failure from mechanical damage. The optical fiber DTS allows for a high density of measurements as well as additional information about the experiment that would otherwise go unmeasured, all with only a single feedthrough. The successful deployment of the optical fiber DTS in the DRIFT experiment campaign is just the first use of a DTS and additional deployments are planned for future experiments.

References

[1] Spencer, B. W., N. E. Woolstenhume, L. A. Emerson, J.-Y. Yeh, D. D. Imholte, C. M. Hill, D. B. Chapman, C. B. Jensen, M. L. Dunzik-Gougar, T. W. Knight, T. M. Besmann, S. Patnaik, S. M. McDeavitt, L. Ortega, D. Perez- Nunez, and H. Ban. 2019. "Separate-effects validation experiments for models of fracture in ceramic nuclear fuel." *In Proceedings of Top Fuel 2019*. Seattle, Washington. September 2019.

[2] Gifford, D. K., B. J. Soller, M. S. Wolfe and M. E. Froggatt. 2005. "Distributed fiber-optic temperature sensing using Rayleigh backscatter," *2005 31st European Conference on Optical Communication*, ECOC 2005. Glasgow. Vol. 3. 2005: 511–512.

[3] Jensen, C., K. Davis, A. Fleming, A. Lambson, K. McCary, K. Tsai, M. Wilding, 2019. *FY19 Report for Instrumentation Development for the Transient Testing Program*. INL/EXT-19-56000. Idaho National Laboratory p., 2019.

[4] Fleming, A., K. McCary, A. Lambson. 2020 . *Development and Testing of Fiber Optic Feedthroughs for In-Pile Applications*. United States: N.

[5] McCary, K., A. Fleming. 2020. *Intrinsic Fiber-Optic Temperature Sensing for Reactor Core Applications*. INL/EXT-21-63231. Idaho National Laboratory.

[6] McCary, K. M., A. D. Fleming, J. E. Daw, S. Rana, H. Subbaranman, and N. Kandadai. 2019. *Out-of-Pile Testing of Radiation Hard Optical Fibers*. INL/EXT-19-54700. Idaho National Laboratory. doi:10.2172/1668371.

Self-Powered Neutron Detector Testing and Characterization in Test Reactors

Kevin Tsai
Idaho National Laboratory

Joe Palmer
Idaho National Laboratory

Troy Unruh
Idaho National Laboratory

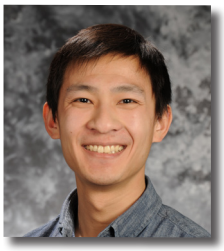

Introduction

Advanced instrumentation enables irradiation testing of nuclear fuels and materials to support deployment of new advanced reactors. This irradiation testing can also provide calibration and validation of state-of-the-art sensors prior to deployment in first-of-a-kind advanced reactors. One of the key parameters to measure in real time is the local neutron flux, in both material test reactor (MTR) irradiation experiments and in newly developed advanced reactors. This parameter is especially crucial in reactors with a widely varied power distribution that limits the accuracy of ex-core detectors; such as the case of the Advanced Test Reactor (ATR) whose unique fuel arrangement allows significant power "tilting" to different regions of the core and conversely for small reactor cores as seen in small modular reactors and microreactors. Therefore, integration of calibrated and qualified in-core neutron flux sensors, as well as their availability as commercial off-the-shelf items, are needed to support irradiation experiments and advanced reactor developers.

Among the various types of in-core neutron flux sensors available, the self-powered neutron detector (SPND) was identified as a strong candidate for deployment in irradiation experiments, as well as for advanced reactor demonstration. The overall goal of the SPND development project within the Nuclear Energy Enabling Technologies Advanced Sensors and Instrumentation (NEET-ASI) program is to identify a clear path towards procuring and qualifying custom-designed and domestically-produced SPNDs that are optimized to function in a wide variety of nuclear environments typical of MTRs and advanced reactor designs.

As a first step towards achieving the overall goal of providing a pipeline of SPNDs manufactured to user-defined specifications, a set of rhodium-based SPNDs were custom designed in collaboration with Idaho Laboratories Corporation. These SPNDs were irradiated alongside miniature fission chambers in a water environment at the Advanced Test Reactor Critical (ATRC) facility. The work was performed synergistically with the ATR I-loop project to measure the effects of an inserted booster fuel/beryllium moderator on adjacent outer irradiation positions in real-time to compare against traditional flux wires measurements (Figure 1) [1].

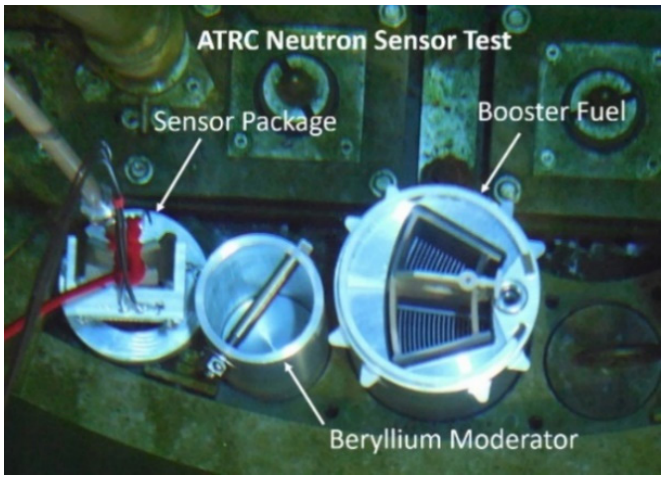

Figure 1: Image of the neutron sensor package, booster fuel, and beryllium moderator in the ATRC I-positions.

Sensor Performance Demonstration in Test Reactors

To verify the functionality of the Rhodium (Rh)-SPNDs prior to its deployment at the ATRC facility, irradiation tests took place at Idaho State University's AGN-201m reactor. The AGN-201m reactor allowed low-flux signal resolution testing at a low electronic-noise environment. Irradiation tests were performed alongside a well-characterized prompt-response Hafnium (Hf)-SPND that acts as a prompt-response flux monitor. The pairing of the prompt and delayed response SPNDs verified the

Continued on next page

Continued from previous page

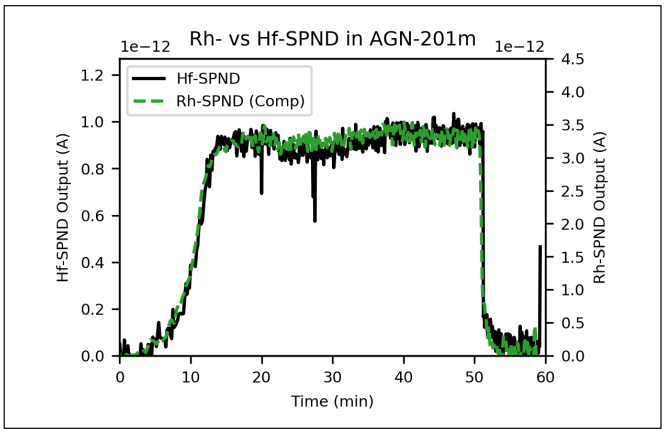

Figure 2: Performance comparison of the Rh-SPND to a Hf-SPND in the AGN-201m reactor.

ability of the Rh-SPND to performed highly resolved measurements at an approximate neutron flux level of 2 × 10^8 n/cm^2-sec, which is near the flux levels expected at the ATRC facility (see Figure 2).

Additional irradiation testing at the Neutron Radiography Reactor (NRAD) reactor was used to demonstrate the sensor response to higher flux levels than achievable at ATRC facility and AGN-201m reactors. Irradiation at NRAD compared the Rh-SPND signals to reactor power in stepped-power changes over five orders of magnitude. The test demonstrated the ability of the Rh-SPND to provide a linear output proportional to reactor power spanning over five decades of reactor power ranging from an estimated neutron flux of 2 × 10^7 n/cm^2-sec to 2 × 10^{12} n/cm^2-sec (see Figure 3 and Figure 4).

After verifying operation, the Rh-SPNDs were deployed in the ATRC facility alongside fission chambers and standard dosimetry (flux wires). Two consecutive irradiations each consisting of 6 hours steady-state operation at 600-W power without and with the fuel booster and beryllium moderator were performed. The fission chambers were incorporated to benchmark the performance of the Rh-SPNDs in both time and signal resolution. Additionally, the dosimetry (flux wires) were incorporated as the standardized flux measurement method that is used to verify the core performance of the booster fuel and beryllium moderator as well as to aid in calibration of the Rh-SPNDs.

Both the U-235 fission chamber as well as the Rh-SPNDs demonstrated excellent performance, as shown in Figure 5, and illustrates the importance of in-core neutron flux sensors by indicating a distinct change in neutron flux. As predicted, the ex-core sensors used to measure overall reactor power were not able to discern the difference between the irradiation without the booster (NB) and with the booster (B); yet each of the in-core flux sensors within the sensor package measured an increase in thermal flux of approximately 20% (see Figure 6).

On-going SPND Characterization

In line with the main objectives of procuring, demonstrating, and characterizing commercially available SPNDs, the dosimetry data obtained from the ATRC facility experiment is currently being used to perform SPND modeling for sensitivity predictions as well as to calibrate the Rh-SPNDs for upcoming

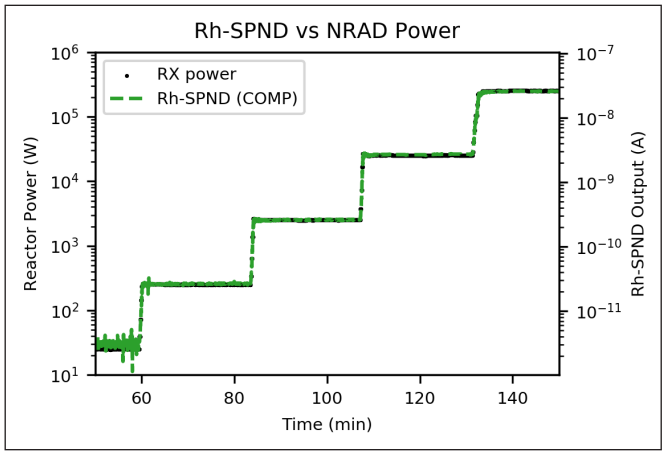

Figure 3. Performance comparison of the Rh-SPND to reactor power at the NRAD reactor.

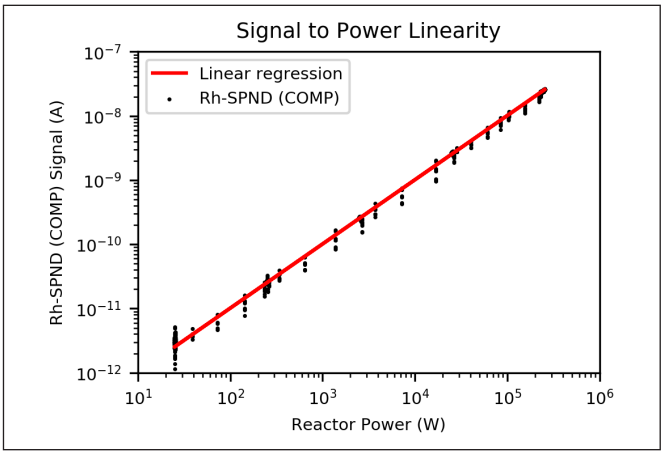

Figure 4. Rh-SPND sensitivity plot on signal linearity to reactor power.

Continued on next page

Continued from previous page

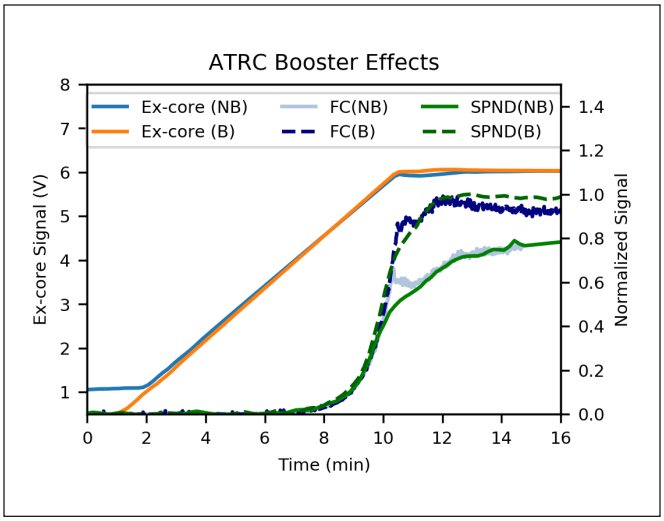

Figure 5. Sensor performance comparison between irradiations in ATRC without and with a booster fuel/beryllium moderator inserted. NB = no booster inserted, B = booster inserted, FC = fission chamber, SPND = Rh-SPND.

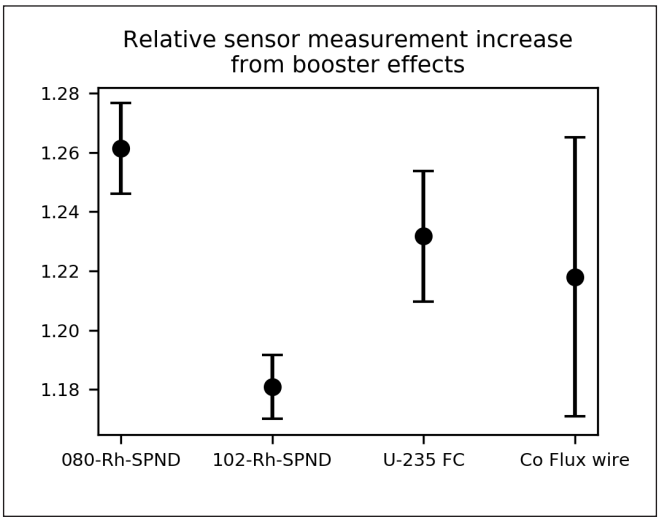

Figure 6. Relative sensor performance on the effects of inserting a booster fuel/beryllium moderator into the ATRC medium I-position.

experiments. Additionally, since many advanced reactor designs operate at high temperatures, upcoming irradiations investigating SPND performance at elevated temperatures will be performed at the NRAD reactor and Massachusetts Institute of Technology Reactor. These results will directly support future SPND designs that are optimized for advanced reactor experiment and operational needs.

Reference:

[1] Means, K., T. Maddock, N. Woolstenhulme, N. Oldham, K. Horman. 2019. "Advanced Test Reactor I-Loop Irradiation Facility and Flux Booster Element," *Transactions of the American Nuclear Society*, vol. 121.

Impedance Sensor Development

Mark Roberson
Goldfinch Sensor Technologies and Analytics LLC

Juliana Pacheco-Duarte
Virginia Tech

Introduction

Detecting and quantifying voids (bubbles) that can form on reactor rods during reactor transients is necessary for producing safer fuel rods. We are developing a void sensor as part of a Small Business Innovated Research (SBIR) Phase II effort. After the current validation phase, we hope to deploy the sensor for use at Idaho National Laboratory (INL). Presently, we are working with colleagues at INL to place sensor elements in the reactor core for high-temperature and neutron exposure testing.

In 2011, a major earthquake induced a 15-meter-high tsunami that struck the Fukushima Daiichi nuclear reactors in Japan. In the ensuing accident, the three operational reactor cores melted down. In response, the U.S. Congress placed an increased emphasis on accident tolerant fuels that could better withstand accidents due to a sudden loss of cooling.

The INL Transient Reactor Test (TREAT) facility uses fast transient tests to simulate reactor accidents in a safe manner. Experiments with fuel rods in water help fuel developers optimize light water reactor (LWR) fuel rod cladding designs. If a void appears on a rod from localized heating, the rod cannot shed heat as efficiently through the air. In a positive feedback effect, the void increases in size and the localized heating becomes more pronounced. Potential resultant issues include cladding cracking and rod failure, so understanding exactly when and where the voids appear is critical.

Goldfinch Sensor Technologies and Analytics (GSTA) successfully completed a Phase I effort to demonstrate the feasibility of using an "impedance sensor" to detect the voids. One consideration in this process included the fact that the impedance of the water is very different from air. This can be visualized when looking at weather radar images in the radio frequency (RF) range and seeing a result of this difference in the form of a rainbow. Other groups have previously suggested the use of impedance measurements to detect voids; however, our approach is unique in the use of varying RF frequencies to take measurements at multiple locations along the rodlet simultaneously. This is essential because there are very few input ports to test chambers, and by multiplexing the signals, we can monitor void formation at more locations than previous approaches. During Phase II, Goldfinch Sensor Technologies and Analytics (GSTA) collaborated with Virginia Tech (VT) for their expertise on the theory of void formation in high-temperature, high-pressure testing.

Objective

The goal of our Phase II effort is to develop and demonstrate direct, time-resolved, multi-position detection and characterization of void formation. This will be conducted in high-pressure, high-temperature environments with minimal electrical feedthrough requirements. Our goal is to deploy sensors in INL irradiations during transient tests and, with fast time resolution, measure accurately when, where, and how the voids form.

We have six task objectives to accomplish in our project, starting with the modeling of the system. The first task involves modeling the electric field created around the sensors (which sense the presence of voids), the RF circuits (because the multiple-frequency device is a complex task in distributed lumped element design), and void formation at the rods. The second project task, led by VT, requires selection, installation and safe operating of an autoclave. The autoclave, operating at a high-pressure and temperature, has significant safety risks if not operated properly, and our VT partner has considerable experience in this field. The third task transitions from the theoretical RF design to the specific element choices, such as deciding between a logarithmic power detector and a phase-sensitive linear power detector. During the fourth task, we will design and build the sensor elements. Unlike a room-temperature design, much of our focus is on the materials and assembly methods necessary to build a sensor, which can detect voids while operating at the high-temperature (900°F), high-pressure (21 MPa), and expected neutron flux levels present in the reactor core. The fifth task focuses on software development, which includes controlling the probing RF electronics and interpreting the sensor response of the probes. We finish out the project with the common Phase II SBIR goal of validating and verifying our technology while documenting our results.

Continued on next page

Continued from previous page

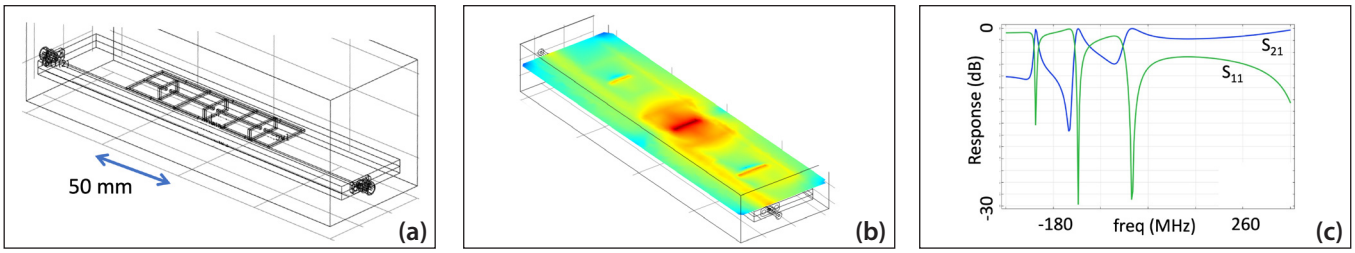

Figure 1. (a) Wireframe view of sensor, (b) Surface plot of $\log(E^2)$, (c) modeled multi-resonator response.

Current Status

Our project has experienced scheduling setbacks due to COVID-19 including a lack of access to GTSA and VT laboratories, as well as delays in product deliveries. We are using the no-cost extension approved by the Department of Energy (DOE) to complete tasks that had supply chain delays. We have also been able to use the new schedule to work with INL in planned tests for survivability in the reactor core.

Currently, we have fully completed half of our subtasks. By the end of 2021, we will have only the subtasks connected to analyzing subsystem testing and final documentation remaining to complete our objectives.

From a computational perspective, the electric field modeling is the most complex part of the work. Near-field electric field simulations [1] in the presence of water are intensive, primarily because the high relative dielectric constant (ε_r) of water. The constant varies with frequency and temperature and is around ε_r=80 at 300 MHz compared to a value of ε_r=1 for air [2]. The large value means that we must work with frequencies below the transverse resonance frequencies (below 300 MHz) of the water-filled test chambers that INL uses for studying void formation on rod claddings. Figure 1 shows a representative model, the modeled electric-field intensity, and the predicted spectrum. We use two separated sensor elements to detect the presence of the void because we can detect voids at a larger distance when compared with only one element. We specifically measure the change in the transmitted power, S_{21}, between Ports 1 and 2. Figure 2 shows a model with two sensor "paddles," a rodlet, and a void. The figure also shows the modeled response and the experimental results for bubble sensing. Presently, our experimental sensitivity exceeds the precision of our modeling.

The number of connectors (feedthroughs) that can go into a TREAT test chamber are extremely limited. While other methods (capacitive plates, for example) can also measure void formation, each of these sensors require a dedicated cable for each sensed location. We have developed the RF circuitry to examine multiple sensor frequencies simultaneously with a single RF feed line, and that change allows us to interrogate many sensors using the two cables (for transmit and receive).

Continued on next page

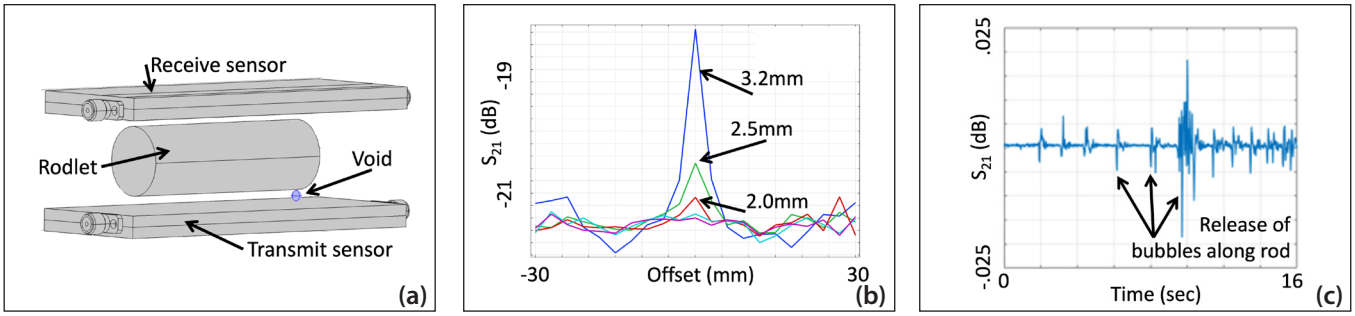

Figure 2. (a) Modeled sensors with rodlet and void (b) Modeled void response vs offset and size (c) Measured response to bubbles on copper rods

Continued from previous page

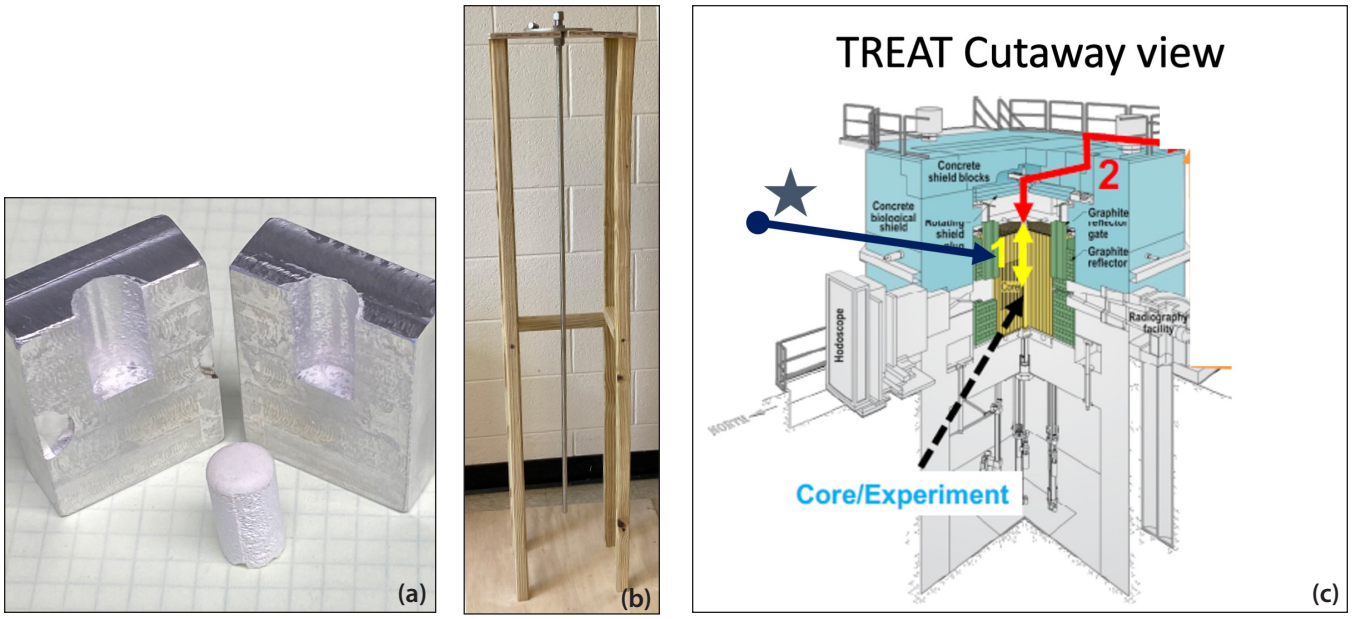

Figure 3. (a) Mold and high-temperature (1650°C, 81 MPa) encapsulant (b) Experiment holder 1.2 m tube in frame (c) Approximate placement area of GSTA-TV1 sensor

Path Forward

We are using the final portion of the Phase II project to conduct testing of the sensing algorithm and the sensor components in a variety of environments and complete all our objectives. We are particularly excited to be able to work with INL in testing our sensor components for survivability in the TREAT reactor [3]. Figure 3 shows an example of a high-temperature encapsulant, our experiment holder design, and the TREAT reactor. Our next step goal is to further commercialize the technology by working with INL in a pilot test for which we plan to apply for a Phase IIB effort. Based on the INL tests, we are considering regulatory pathways for the commercial nuclear fleet and licensing the technology. We are also exploring faster time-to-market opportunities in other applications with fewer regulatory requirements.

Conclusion

GSTA is validating and verifying a rodlet void sensor with an end-goal of transitioning the sensor for use by INL. The modeling and experimental results show that the technology works and we are working to validate the sensor for use in the challenging conditions of the INL TREAT facility.

Acknowledgements

GSTA wishes to thank DOE for providing commercialization assistance as part of the SBIR program. The Larta team, and in particular Gunjan Siroya, our principal advisor, have helped us develop a realistic go-to-market and commercialization strategy for the SBIR technology. We also wish to thank INL for their collaborative help, as we have benefitted tremendously during the program because of the INL staff. We would like to thank Colby Jensen, Nic Woolstenhulme, Kevin Tsai, and Pattrick Calderoni for multiple technical discussions and the many technical and administrative staff who have made previous and future visits to the TREAT facility possible.

References

[1] Comsol. 2021. www.comsol.com . Webpage accessed August 6, 2021.

[2] Vijay, R., R. Jain, and K. S. Sharma. 2015. "Dielectric Properties of Water at Microwave Frequencies." *Int. J. Eng. Res. Technol*. 3. no. 03.

[3] Jensen, C., K. Tsai, and A. Fleming. 2020. *FY20 Report for Instrumentation Development for the Transient Testing Program*. INL/EXT-20-59951. Idaho National Laboratory. September 2020.

Development of an Optical Fiber Based Gamma Thermometer

Thomas E. Blue: *Project PI*
The Ohio State University

Pavel Tsvetkov: *Collaborating Org. PI*
Texas A&M University

Diego Mandelli: *Collaborating Org. PI*
Idaho National Laboratory

Anthony Birri: *Student*
The Ohio State University

Joshua Jones: *Student*
The Ohio State University

Tyler Gates: *Student*
Texas A&M University






Introduction

The purposes of our project are to (1) develop an Optical Fiber–Based Gamma Thermometer (OFBGT) that is appropriate for use in University Research Reactors (URRs); (2) test the OFBGTs in two University Research Reactors, namely the Ohio State University Research Reactor (OSURR) and the Texas A&M Research Reactor (TAMURR); and (3) develop methods to calculate the volumetric power distribution (and its associated uncertainty) within a URR from the data that is produced by an array of OFBGTs. These goals are intended to be first steps in the development of OFBGTs for application in power reactors.

The rationale for this research project is discussed below with regards to the application of OFBGTs in Boiling Water Reactors (BWRs) for which Gamma Thermometers (GT) that use thermocouples to sense temperatures have been deployed. (Herein, we will call GTs, which use thermocouples, state-of -the-art GTs [SOA GTs] to distinguish them from the OFBGTs that we are developing). The volumetric power distribution in BWRs is monitored by local power range monitoring (LPRM) systems. Over time, the LPRM systems lose sensitivity due to burnup of the fissionable material and needs recalibration. SOA GTs provide a permanent system of sensors for LPRM calibration that do not degrade by burnup. A SOA GT is composed of an isolated thermal mass, an outer sheath, and a gap between the thermal mass and the sheath. The SOA GT temperature (the temperature of the thermal mass) is monitored by a thermocouple, and a second thermocouple, conceivably, is used to monitor the temperature of the outer sheath. A temperature difference, ΔT, is generated between the thermal mass and outer sheath, as a result of the thermal resistance of the gap. Assuming that the relationship between energy deposition rate and ΔT is known, one can acquire a dose rate measurement in the SOA GT. The dose rate measurement in a given SOA GT can be used to calibrate an adjacent LPRM.

A system of SOA GTs for LPRM calibration could be improved by making them optical fiber-based [1] (i.e., by making them OFBGTs). Utilizing optical frequency domain reflectometry (OFDR), one can acquire a distributed temperature measurement along an optical fiber, thus one can monitor the temperature of a linear array of OFBGTs with the same fiber. That linear array of OFBGTs, which we call simply an OFBGT, is designed to extend the length of an instrument tube of a reactor, and could acquire multiple dose rate measurements along the length of the instrument tube.

An OFBGT has been designed, constructed, and tested by the collaborating institutions on this project. In addition, the collaborators on this project have developed a data analytic methodology that allows one to infer the power distribution in a reactor core, based on the response of an array of OFBGTs in the core, thus making the OFBGT technology promising for application in many reactor types and not just for LPRM calibration in BWRs. Details of the data analytic methodology can be found in a previous publication [2]. To date, we have tested two OFBGTs in the OSURR and are in the process of testing two OFBGTs in the TAMURR.

Overall Design Description

The OFBGT design is shown in Figure 1. The overall OFBGT design can be broken down into three main parts: the thermal mass, the gas gap, and the outer sheath. Gamma rays (and to a lesser extent neutrons) deposit energy, within the thermal mass, with a linear energy deposition rate q_γ. The gas gap provides the dominant thermal resistance out of the three OFBGT regions. We call this resistance R. A temperature difference, ΔT, is generated across the gas gap between the thermal mass and the outer sheath, as described by:

$$\Delta T = q_\gamma R \qquad (1)$$

Continued on next page

Continued from previous page

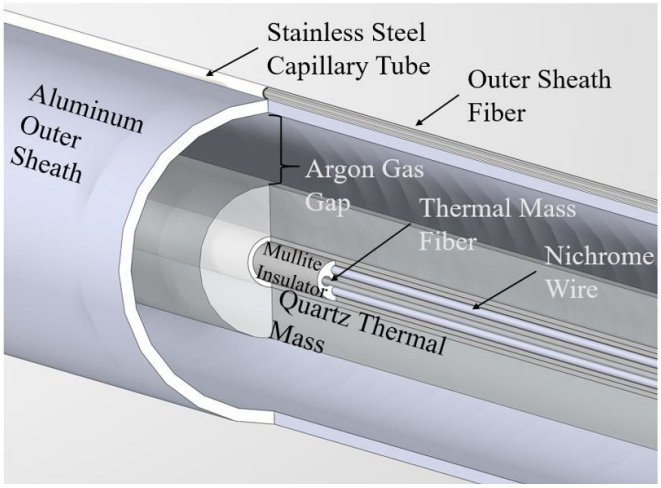

Figure 1. Depiction of the OFBGT design.

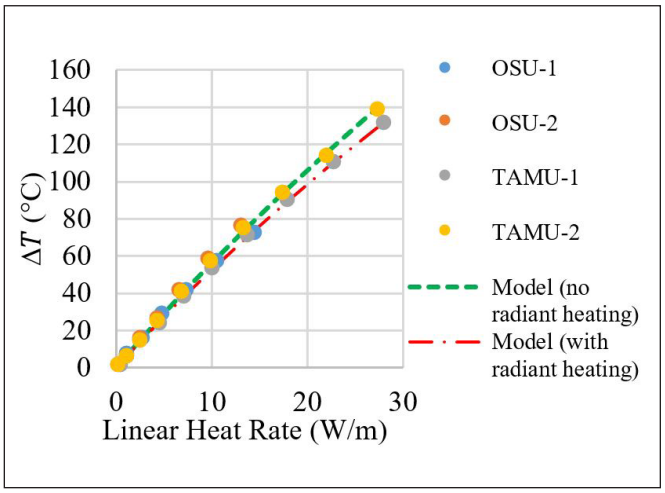

Figure 2. Calibration results of the OFBGTs shown with thermal modeling results.

The bulk of the thermal mass is a thick quartz glass tube. Within the quartz tube is a mullite insulating tube with four through-holes. Within two of the through holes are two optical fibers (one in each through-hole). A nichrome heating wire travels down the thermal mass and back up the thermal mass, within the other two through-holes. The nichrome wire is used to calibrate the OFBGT, by supplying a known range of linear energy deposition rates, q, thus allowing us to develop a relationship between ΔT and a surrogate for q_v. The gap between the mullite insulator and the quartz thermal mass is filled with silica powder, to enhance heat transfer between these two components. The gas gap is composed of argon. The outer sheath is constructed of aluminum 5052, and the temperature of the outer sheath is monitored by an optical fiber within a stainless steel capillary tube that is bonded to the outer sheath. The outer diameter of the OFBGT is 0.5 inches.

Calibration Results

Four OFBGTs have been constructed and calibrated. Two of these OFBGTs have been tested at the OSURR, and are thus named the OFBGT-OSU-1 and the OFBGT-OSU-2. The other two OFBGTs are currently being tested at the TAMURR, and are named the OFBGT-TAMU-1 and the OFBGT-TAMU-2.

The calibration was achieved by having the OFBGTs fit within a vertical water tube with an inlet at the top and an outlet at the bottom. A Haake water heater/circulator was used to supply pump pressure that forces flow through the water tube, allowing the water to have a spatially uniform and temporally constant (but adjustable) temperature. A power supply was utilized to provide a range of currents and hence, q, to the OFBGTs during calibration.

From the experimental calibration, the resultant relationship between ΔT and q for all four OFBGTs is shown in Figure 2, along with two different analytic thermal models for comparison with the experimental data. One thermal model considers radiant heating, while the other does not. The agreement between measurements and calculations is very good, when radiant heating is included in the models. Sensor-to-sensor discrepancies may be due to (1) different packing factors of the silica powder from OFBGT to OFBGT, and (2) different oxidation levels on the inside of the outer sheath from OFBGT to OFBGT, causing different outer sheath emissivity values.

Reactor Experiment Results

The OFBGT-OSU-1 and the OFBGT-OSU-2 have been tested separately, in the water irradiation facility (WIF) of the OSURR. The WIF is in a peripheral location of the reactor core. The OFBGT-OSU-2 is shown within the WIF of the OSURR in Figure 3.

The OFBGT-OSU-1 was constructed and tested prior to the construction and testing of the OFBGT-OSU-2. As such, design flaws that were discovered in the OFBGT-OSU-1, which resulted in a poor sensor performance, were fixed for the OFBGT-OSU-2. A couple of these design flaws included (1) improperly located centering spacers for the thermal mass, which resulted in localized heat loss in the

Continued on next page

Continued from previous page

effective sensor region; and (2) use of a coated fiber, which caused a strain on the fiber, thus adding an error to the OFDR-based temperature measurements. The OFBGT-OSU-2 has more strategically placed centering spacers, and utilizes stripped fiber in the effective sensing region.

The normalized linear heat rate in the OFBGT-OSU-2 is shown in Figure 4. The profile is shown for t=21 min, and t=58 min after full power was achieved. The theoretical profile, calculated with MCNP, is also shown in Figure 4. One can see that the experimentally acquired profile at t=21 min more closely resembles the theoretical profile than the experimental profile at t=58 min. This may be due to experimental error that relates to an added strain of the fiber, or a change in the volumetric power profile of the reactor from t=21 min to t=58 min. The nature of the experimental data in Figure 4 is still being investigated.

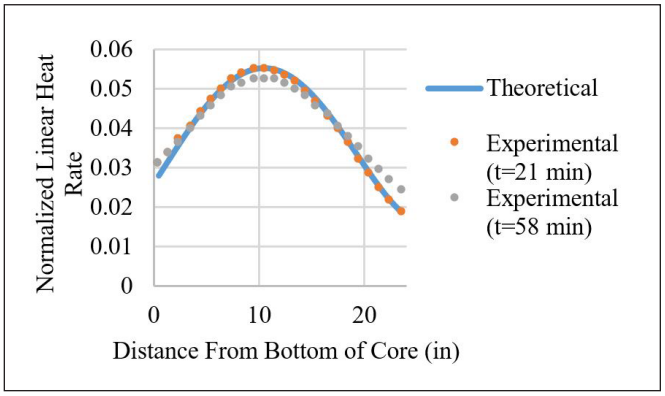

Figure 4. Measured normalized linear heat rate to the OFBGT-OSU-2 compared with MCNP data.

Conclusions

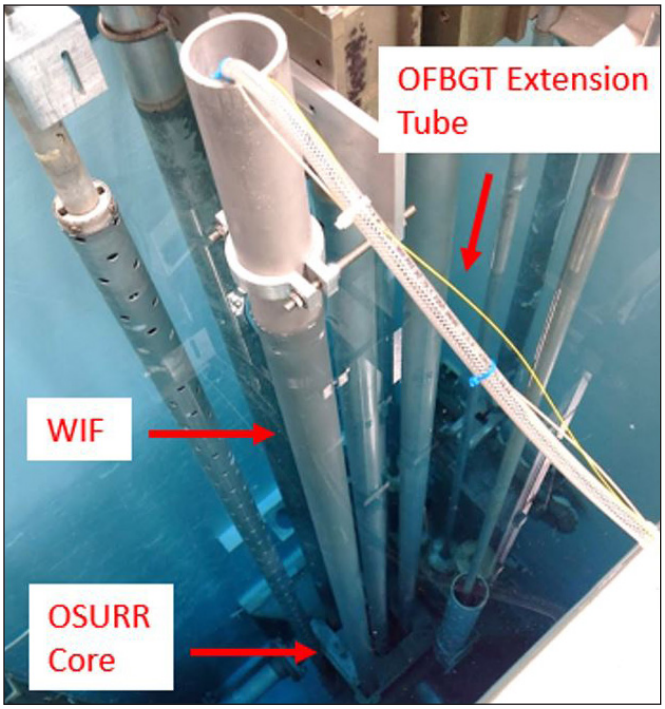

Figure 3. OFBGT-OSU-2 within the OSURR.

The ability to measure a distributed gamma-ray dose rate has been demonstrated with an OFBGT in the OSURR. Demonstration of this capability is an ongoing effort at the TAMU TRIGA. Design flaws were discovered in the OFBGT-OSU-1, which led to improvements in the subsequently constructed OFBGTs, and moreover the realization of key design features that the OFBGT must possess. The experimentally acquired data from the OFBGT-OSU-2 may be used to infer the core power distribution using [2].

Our future plans include completing testing at the TAMURR, using OFBGT-TAMU-1 and OFBGT-TAMU-2, which have already been constructed; but which need to be modified to more firmly secure their capillary fibers to their outer sheaths. In addition, we intend to build and test a high-temperature capable OFBGT that uses single crystal sapphire optical fiber, with readout by an OFDR, for temperature sensing.

References

[1] Koste, G. P., H. Xia, K. Lee. 2013. "Optical Gamma Thermometer." Patent No.: U.S. 8.503,599 B2.

[2] Birri, A., T. E. Blue. 2020. "Methodology for inferring reactor core power distribution from an optical fiber based gamma thermometer array," *Progress in Nuclear Energy*, 130: 103552.

Analytics-at-scale of Sensor Data for Digital Monitoring in Nuclear Plants

Cody Walker
Idaho National Laboratory

Vivek Agarwal
Idaho National Laboratory

Nancy Lybeck
Idaho National Laboratory

Pradeep Ramuhalli
Oak Ridge National Laboratory

Mike Taylor
Electric Power Research Institute

Introduction

The domestic fleet of light water reactors are facing economic sustainability challenges in the current energy market that are causing premature closures of nuclear power plants despite their excellent safety records. Preventative maintenance is one of the contributors to the high operating costs of the domestic fleet. Transformational advancements in sensors, communications, big-data analytics, machine learning, and artificial intelligence technologies must be leveraged to ensure the transition to a predictive-maintenance strategy. The scope of this ongoing research is to develop and validate machine-learning-based technological solutions to address the technical gaps and challenges in achieving digital monitoring in nuclear plants. Digital monitoring capabilities leverage advancements in the mentioned areas to enable a cost-effective predictive-maintenance strategy for nuclear plants. The overall scope of the ongoing research is shown in Figure 1.

To achieve digital monitoring, the project has performed research and development to:

1. Design a multi-band heterogeneous network architecture that can support automation of a wide variety of plant applications ranging from low- to high-power, low- to high-frequency, and short- to long-range communication regimes. A generalized formulation has been developed to determine technical and economic feasibility via techno-economic analysis (TEA) [1].
2. Identify and recommend installation of wireless vibration sensor technologies capable of transmitting data over different communication protocols. This enabled collection of data that was previously not collected [2].
3. Develop machine-learning techniques for condition estimation and maintenance decision making using structured and unstructured heterogenous data distributed across space and time (i.e., analytics-at-scale). The developed diagnostic and prognostic models are used to identify potential faults and estimate time to reach an alarm limit, allowing advanced planning for the system of interest to be taken out of service for maintenance [3, 4].
4. Develop guidance on data and information visualization using different tools to ensure the right actionable information is made available to the right person, in a useful format, at the right time [5].

Digital Monitoring and Machine-Learning Analytics

To achieve the research scope (Figure 1), the above-mentioned research advancements progressively build on one another to address current technological gaps to enable digital monitoring of nuclear plant equipment. Prior to recommending installation of new sensor technologies for asset monitoring, insights into a technology's feasibility, cost, benefits, risks, and uncertainties related to new sensor technologies need to be evaluated. The TEA formulation was developed to aid the deployment of wireless sensor technologies in nuclear power plants. The TEA formulation provided the ability to evaluate technical and economic feasibilities of wireless network architectures (such as distributed antenna systems, wireless local area networks, and other technologies) supporting wireless vibration sensor deployment [1].

Continued on next page

Continued from previous page

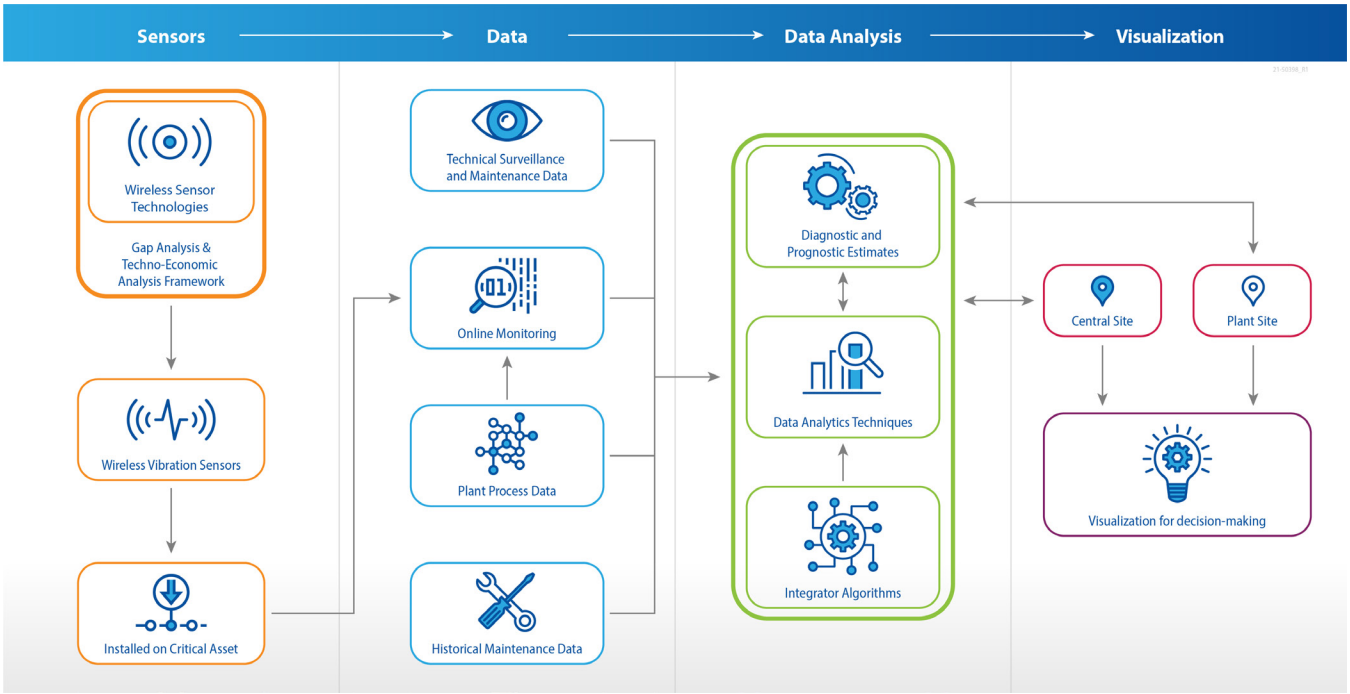

Figure 1. Research scope enabling digital monitoring at nuclear power plants through advancements in sensors, communications, and machine-learning technologies.

The feedwater and condensate system from both boiling-water and pressurized-water reactors was selected for digital monitoring and development of tools to enable use of a predictive-maintenance strategy. A wide range of data was already being collected at different spatial and temporal resolutions on the feedwater and condensate system. The existing plant process data related to the feedwater and condensate system includes temperature at different locations, pressure, flows, and gross load. In addition to existing data, a recommendation was made to the plant sites, based on the TEA, to install wireless vibration sensors on the feedwater and condensate system. The monitoring data was made available to Idaho National Laboratory by collaborating nuclear plant sites. In addition, the maintenance logs (i.e., work orders) that capture the tasks that were completed, either to repair equipment or as part of preventative maintenance, were also made available. These data were analyzed to develop diagnostic and prognostic models [3, 4] using machine-learning techniques, setting the case for analytics-at-scale.

Figure 2 shows application of a developed condition indicator in identifying a sensor drift. The condition indicator identified an abnormally high temperature by comparing the component's current temperature with its seasonal average to diagnose a sensor drift that was fixed during the next outage. This indicator was combined with other indicators (also referred as features) using principal component analysis. The generated feature space was used to train three machine-learning algorithms for short-term forecasting of equipment condition: Long short-term memory neural networks, support vector regressions, and random forests. Here, short-term forecasting provided insight on expected equipment condition 1 hour, 1 day, and 1 week into the future. Work has been performed to improve the input feature selection process through use of Shapley additive explanations and variance inflation factors.

In addition to analyzing process data, the maintenance logs for major components within the feedwater and condensate system (condensate pumps, condensate booster pumps,

Continued on next page

Continued from previous page

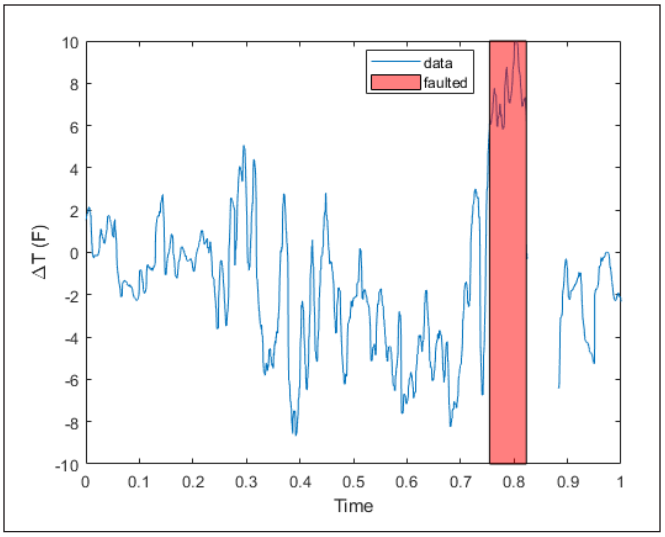

Figure 2. Identification of a sensor drift fault through a developed condition indicator (the axes values are normalized and anonymized to protect plant information).

their respective motors, etc.) were also analyzed to assess equipment health. Based on the equipment's historical health condition, recommendations were provided to update the frequency of certain preventative-maintenance tasks, such as oil analysis and refurbishments. The recommendations aligned with the recommended frequencies within the Electric Power Research Institute Preventative Maintenance Basis Database, which contains maintenance frequencies from across several industries and utilities.

Given heterogeneous data are used to extract information regarding equipment condition using machine-learning models, it is important to present data and information to different users for informed decision-making. To ensure consistency and prevent information overload to the human in the loop, research was performed to standardize visualization requirements that are portable across different visualizations tools. Some of these visual considerations include colors, saliency, information density, patterns, and guided attention. This allows highlighting and grouping the consequential data efficiently so that actionable information is provided to the target user [5].

Summary and Path Forward

This research has advanced the state-of-the-art for online monitoring of nuclear power plant assets and supports the Department of Energy's goals of economic long-term operation of existing light water reactors. Using online monitoring, machine learning, and information visualization, the industry can begin to transition from a preventative-maintenance strategy to a more economical predictive-maintenance strategy. As part of path forward, the project team is working on validating the developed methods and models on a data set from an independent plant

References

[1] Manjunath, K. A., and V. Agarwal. 2020. "ISM band Integrated Distributed Antenna Systems for Industry 4.0: A Techno-Economic Analysis," *GLOBECOM 2020 - 2020 IEEE Global Communications Conference*. 1–6. doi: 10.1109/GLOBECOM42002.2020.9322617.

[2] Agarwal, V. 2020. *Wireless Sensor Modalities at A Nuclear Power Site to Collect Vibration Data*. INL/EXT-20-58548. Rev 0. Idaho National Laboratory. June 2020.

[3] Walker, C., P. Ramuhalli, V. Agarwal, and N. Lybeck. 2021. "Nuclear Power Fault Diagnostics and Preventative Maintenance Optimization." *12th Int. Top. Meet. Nucl. Plant Instrumentation, Control. Human-Machine Interface Technol. NPIC HMIT 2021*. June 14–17.

[4] Ramuhalli, P., C. Walker, V. Agarwal, and N. Lybeck. 2021. "Nuclear Power Prognostic Model Assessment for Component Health Monitoring." *12th Int. Top. Meet. Nucl. Plant Instrumentation, Control. Human-Machine Interface Technol. NPIC HMIT 2021*. June 14–17.

[5] Mortenson, T., T. Miyake, and R. Boring. 2021. *Data Visualization to Support Decision Making at Nuclear Power Plants*. INL/EXT-21-62703. Rev 0. Idaho National Laboratory. May 2021.

Zero-Group-Velocity Method for Microstructure Characterization

Robert Schley
Idaho National Laboratory

Zilong Hua
Idaho National Laboratory

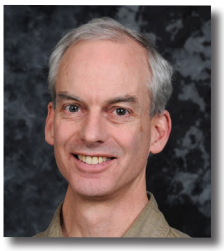

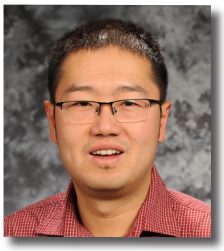

Motivation and Background

Properties of nuclear fuels change dramatically during reactor operation, primarily due to the generation and evolution of microstructural defects resulting from irradiation at temperature extremes. Cataloguing these processes experimentally is required for rapid validation and verification of advanced fuels and materials. This work focuses on the development of unique instruments that can overcome the challenge introduced by reactor extremes, including high temperatures, high radiation fields, and limited access. Our previous efforts have led to successful tests that monitor the change in mechanical property of small cantilever beam samples at the Idaho National Laboratory's (INL's) Transient Reactor Test Facility (TREAT) [1]. While a cantilever beam geometry is convenient for instrumentation consideration, the extrinsic mechanical coupling to the environment through the cantilever boundary restricts the ability to perform measurement of acoustic attenuation caused by interaction of ultrasound with microstructure. Zero-Group-Velocity (ZGV) Lamb wave measurements, which are evanescently damped in the lateral direction of a plate, are expected to greatly reduce extrinsic attenuation caused by coupling to the environment and enable connecting intrinsic attenuation measurements to microstructure.

Methodology

Lamb waves are elastic wave modes guided in a thin plate sample. Infinite Lamb wave modes coexist in each plate, and ZGV Lamb mode plate waves are formed from the interference of two spatially counterpropagating Lamb waves with unique combinations of frequency and wave number. The mechanical energy carried by a ZGV plate wave is locally trapped, and the evanescent ZGV plate wave is thus insensitive to the lateral boundary conditions [2]. A comparison of a mechanical wave vs a ZGV plate wave is illustrated in Figure 1.

Measurements of ZGV plate waves at room temperature and high temperature on several reference materials were accomplished using the recently developed Material Properties Microscope (MPM). With promising results obtained, similar measurement was conducted on a metallic nuclear fuel, uranium-molybdenum (U-10Mo). The MPM is an instrument developed at INL as a test bench to facilitate the development of new laser ultrasound measurement methodologies. The MPM incorporates a train of short-duration laser pulses (Quantel Ultra Q-Switched Nd: YAG) for ultrasound excitation and a laser interferometer (Bossa Nova TEMPO500 photorefractive interferometer) for ultrasound detection. A Linkam model TS1000V heating stage is used for the high-temperature measurements up to 1000°C.

Continued on next page

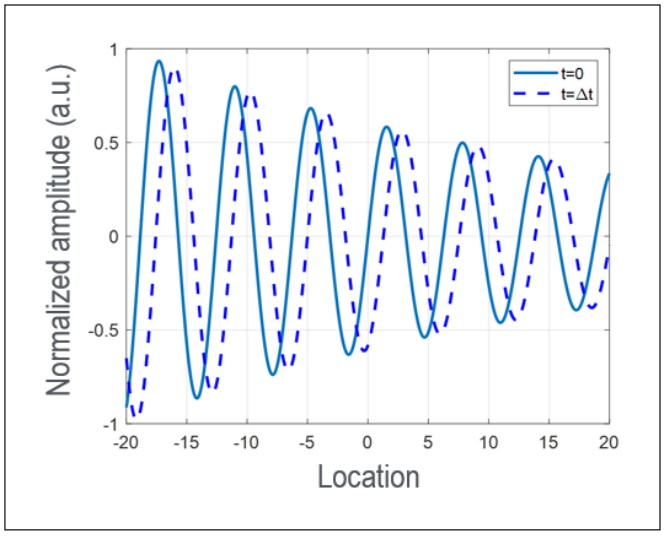

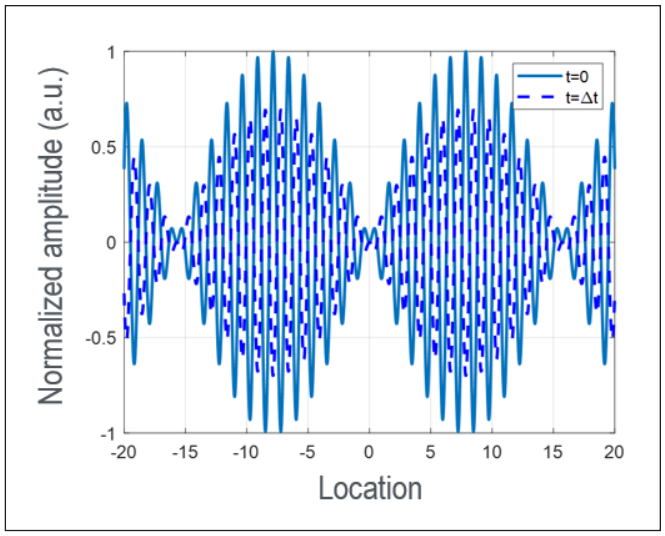

Figure 1. Mechanical wave (left) vs ZGV plate wave (right). Note that the group velocity of mechanical wave is non-zero, and the overall wave is moving to one direction; and for ZGV plate wave the overall waveform is trapped locally.

Continued from previous page

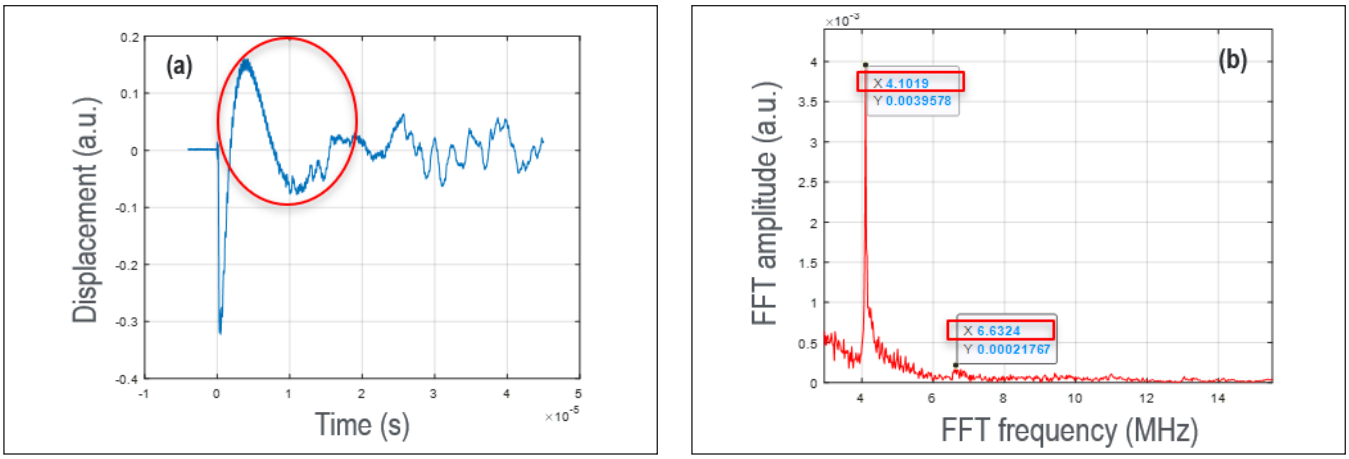

Figure 2. Experimental data of ZGV measurement on brass. (a) raw data, with the ZGV plate wave observed as highlighted in the red circle; (b) frequency spectrum after Fourier transformation, with the frequency peaks of first and second ZGV modes identified in the red boxes.

Current Status

As several acoustic waves can be simultaneously excited, the Rayleigh-Lamb equations were modeled using MATLAB to confirm the observation of ZGV plate waves. The frequency values of the ZGV plate waves from the experiment were compared to the values from the model prediction to validate the measurement approach. Room-temperature measurements have been conducted on five samples: two aluminum (Al) alloys with different thicknesses, tungsten (W), brass, and single crystal silicon (Si). Raw experimental data in the time domain and the corresponding spectrum of ZGV wave frequencies on brass are shown in Figure 2, as an example, and results on all samples are summarized in Table 1. Two ZGV wave modes were captured on all samples, with the first ZGV wave amplitude significantly higher than the second. The real plane dispersion curves calculated from modeling are given in Figure 3, with the two experimentally observed modes highlighted. As the figures and table show, the ZGV plate wave frequencies from measurement match the modeling calculation closely, with the difference no more than 2.1%.

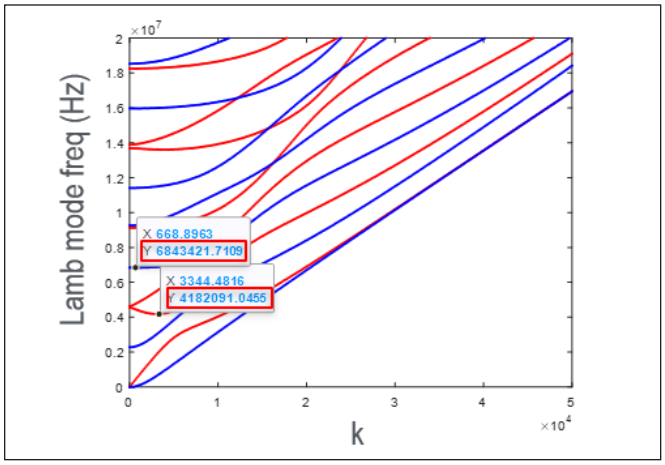

Figure 3. The real plane dispersion curves of Lamb wave from modelling. Two ZGV Lamb waves observed on brass were identified as S3 (third S-mode represented by blue curves) and A2 (second A-mode represneted by red curves). The ZGV wave frequencies are highlighted in red boxes, which agree closely to the experimental results in Table. 1.

Table 1. Summary of ZGV plate wave measurement results at room temperature, and corresponding calculation results. The experiment-modelling difference of the 1st ZGV pate wave frequency is generally smaller than ~2%.

Material	ZGV frequency - experiment [MHz] (1^{st}/2^{nd})	ZGV frequency - modelling [MHz] (1^{st}/2^{nd})	frequency difference (1^{st})
Al alloy 1	3.72/12.20	3.71/11.97	0.27%
Al alloy 2	5.27/13.37	5.24/16.95	0.57%
W	4.86/8.48	4.89/8.62	-0.61%
Brass	4.10/6.63	4.18/6.84	-1.91%
Si	6.41/11.8	6.28/12.28	2.07%

Continued on next page

Continued from previous page

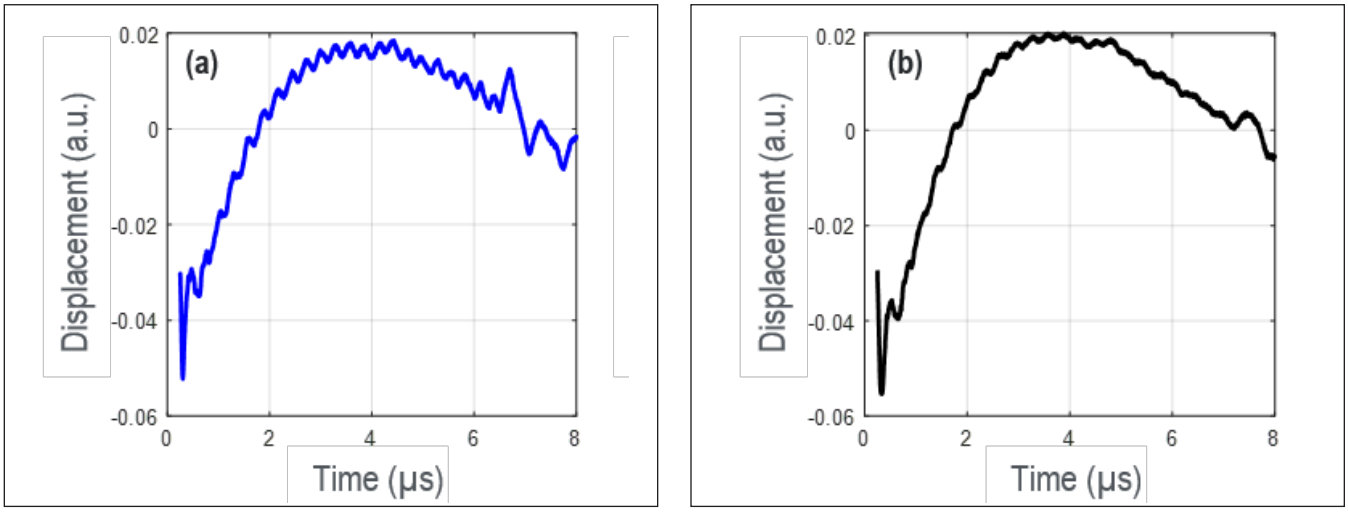

Figure 4. ZGV wave measured on Cu at (a) 25˚C and (b) 700˚C. Note the waveform amplitude reduction at high temperature.

A new set of reference materials, copper (Cu), molybdenum (Mo), W, and Si, were carefully prepared to validate the high-temperature ZGV wave measurements in the temperature range from 25°C to 1000°C. Similar variation trends of ZGV plate wave amplitude and frequency with respect to temperature were obtained on all samples from both raw experimental data in the time domain (Figure 4) and post-processed frequency spectrum in the frequency domain (Figure 5). The example material in the figures is Cu. The reduction of ZGV plate wave amplitude can be clearly seen from comparing the waveform at 25°C to at 700°C. The frequency of first ZGV wave also shifts from 3.54 MHz at 25°C to 3.16 MHz at 700°C. The frequency shift is primarily related to the Young's Modulus dependence on temperature, and the amplitude reduction is likely caused by the increase of internal friction [3].

Lastly, high-temperature measurements were made on a surrogate nuclear fuel sample (U-10Mo) in the temperature range of 25°C to 800°C. The less than ideal surface condition was found to significantly reduce the signal-to-noise ratio of the ZGV waveform, making it difficult to accurately determine the ZGV plate wave frequency (a small peak was still found at approximately 1.35 MHz). Instead, the cross-plane longitudinal wave, which has a better tolerance to the poor surface condition, was captured. Calculated from the velocity of the cross-plane longitudinal wave, a plot of Young's Modulus versus temperature indicates a slight slope change at the temperature of approximately 550°C, indicating the phase transformation (the literature value of this phase change is 570°C).

The next steps in this work include repeating the ZGV plate wave measurement on the same sample with a better prepared surface. General optimization to improve the signal-to-noise ratio of ZGV plate wave measurements will also be investigated. This will enable the characterization of the acoustic damping, which provides unique insights into the interaction of ultrasonic waves with microstructural defects (e.g., grain boundaries, point defects, and dislocations).

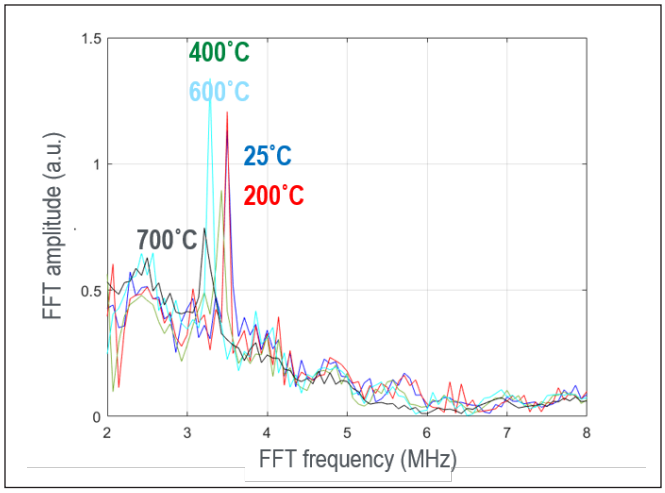

Figure 5. Frequency spectrum of the 1st ZGV plate wave on Cu. From 25˚C to 700˚C, the wave frequency is reduced from 3.54MHz (blue curve) to 3.16MHz (dark curve), and the peak magnitude also generally reduces (with 600˚C as an exception).

Reference

[1] Schley, R. S., L. K. Aagesen Jr, Z. Hua, D. H. Hurley. 2019. *Detailed Analysis of RUS Insertion Experiment and Scoping Studies for Performing Next Experiment using an Enriched Fuel Sample*. INL/EXT-19-55962. Idaho National Laboratory.

[2] Yan, G. "Zero-group-velocity Lamb modes in laser ultrasonics: fatigue monitoring and material characterization," *Le Mans*. 2018.

[3] Blanter, M. S., I. S. Golovin, H. Neuhauser, H. Sinning. 2007. *Internal friction in metallic materials, A Handbook*. 540: 1–144.

16-50050-15R5